Superlattices and Microstructures 109 (2017) 145–153

Contents lists available at ScienceDirect

Superlattices and Microstructures

journal homepage: www.elsevier.com/locate/superlattices

Growth, mechanism and properties of TiO_2 nanorods embedded nanopillar: Evidence of lattice orientation effect

M. Jithin [a], K. Saravanakumar [a, *], V. Ganesan [b], V.R. Reddy [b], P.M. Razad [a], Manju Mishra Patidar [b], K. Jeyadheepan [c], G. Marimuthu [a], V.R. Sreelakshmi [a], K. Mahalakshmi [d]

[a] Department of Physics, Kongunadu Arts and Science College, Coimbatore, 641029, India
[b] UGC-DAE Consortium for Scientific Research, Khandwa Road, Indore, 452017, India
[c] Multifunctional Materials & Devices Lab, SASTRA University, Thanjavur, 613401, India
[d] Department of Physics, Providence College for Women, Coonoor, Nilgiris, 643101, India

ARTICLE INFO

Article history:
Received 9 January 2017
Received in revised form 24 April 2017
Accepted 26 April 2017
Available online 27 April 2017

Keywords:
Epitaxial nucleation
TiO_2 nanotent
TiO_2 nanorod
TiO_2 nanopillar

ABSTRACT

Worldwide researchers and scientists are taking efforts to develop novel structured highly crystallized nanomaterials to fabricate devices for various applications. In this report, we demonstrate the synthesis of self-originated single phase Titanium dioxide (TiO_2) nanorods embedded nanopillar on nanotent grain under simple hydrothermal method. Synthesized TiO_2 nanopillars are in single crystalline tetragonal crystal structure with rutile phase. Understanding the fundamental crystal nucleation and growth mechanism is more critical in the semiconducting oxide thin films with controlled size and morphological features. The growth mechanism of TiO_2 nanopillars on the surface of Fluorine doped Tin Oxide (FTO) substrate is explained in support of FESEM and AFM images. The optical emission properties are studied with photoluminescence spectroscopy.

1. Introduction

During past few decades, Titanium dioxide (TiO_2) is given considerable attention from researchers because of its broad applications in photovoltaic devices [1–3], sensors [4] and photocatalysis [5,6]. In photovoltaic devices, one-dimensional (1D) TiO_2 nanostructures such as nanowire, nanorod and nanotube are playing an insuperable role. TiO_2 1D nanostructures show significant efficiency than other dimensional TiO_2 nanostructures in dye-sensitized solar cells (DSSCs) [7,8] and photoelectrochemical cells [9] because those are offering a direct electric pathway for photo-generated electrons [10]. The single crystalline nature and phase of the materials are enhancing the electron transport rate [11]. In DSSCs, rutile TiO_2 has many advantages comparable to anatase phase; it includes a higher refractive index and better chemical stability [12,13]. From these reasons, it is imperative to identify the effect of novel structured 1D TiO_2 to enhance the photovoltaic efficiency. Conversely, the synthesis of single phase 1D TiO_2 nanostructure on a substrate remains a significant challenge [14]. Currently, many methods are available to synthesize 1D TiO_2 nanostructures. The solution-based approaches are more suitable for inexpensive mass production than vapour-phase methods. In those traditional solution-based deposition methods, a hydrothermal method is quite attractive, since it applies to the different type of substrates and it suppresses the fatal crystallographic

* Corresponding author.
E-mail address: dr.k.saravanakumar@gmail.com (K. Saravanakumar).

http://dx.doi.org/10.1016/j.spmi.2017.04.046
0749-6036/

defects even in lower temperatures [15]. However, the controlling of particle size, diameter, length and spatial location of the particle is infeasible in hydrothermal synthesis [16]. Various 1D nanostructured TiO_2 thin films were already synthesized by hydrothermal technique and has been studied by several researchers, giving considerable attention for fabricating novel structures to explore the changes in properties concerning quantum confinement [17–19]. It is a critical and challenging task to investigate the elementary science behind the mechanism of growth of nanostructures from the atomic level.

Herein, we report the novel synthesis of single-crystalline rutile phase TiO_2 nanopillars consisting of TiO_2 nanorods on TiO_2 nanotents in the surface of FTO substrate via the simple hydrothermal method. The fundamental growth mechanism, morphology, structure and optical properties are investigated in detail.

2. Experimental details and characterization tools used

TiO_2 nanorods were synthesized by hydrothermal method using 50 ml Teflon-lined stainless steel autoclave. FTO/glass (1 cm × 2 cm) systematically cleaned with acetone, ethanol and deionized water (DI) in ultrasonic agitator for 20 min and drying in air at 100 °C temperature were used as the substrates. Titanium (IV) isopropoxide (TTIP) was used for titanium source and water with hydrochloric acid (HCl) was used as the solvent. TTIP was dissolved in the mixture of water and concentrated HCl. The cleaned FTO substrates were kept at an angle of 45° from the wall with the conducting side of FTO substrates facing down in a 50 ml Teflon liner; the precursor solution was poured into it. The Teflon liner with the precursor solution was placed into a stainless steel autoclave and kept inside the controlled furnace. The hydrothermal synthesis was performed at 160°C for 2–8 h. After cooling down to room temperature, the samples were rinsed with DI water and dried in ambient condition. Four numbers of samples were prepared with various TTIP amounts as 0.05 ml, 0.10 ml, 0.15 ml and 0.20 ml are named as A, B, C and D respectively.

Various characterization tools were used to investigate the properties of thin films. The structural characterization and phase purity analysis were done using gracing incident X-Ray diffraction (GIXRD) and Raman spectroscopy. The surface morphological analysis was performed using field emission scanning electron microscopy (FESEM) and atomic force microscopy (AFM). The optical analysis was performed using Photoluminescence spectroscopy (PL).

3. Results and discussion

3.1. Structural investigations

The GIXRD pattern of synthesized TiO_2 nanostructures for various quantities of TTIP is shown in Fig. 1. All diffraction peaks confirm the single crystalline tetragonal crystal structure with rutile phase of TiO_2 ($P4_2/mnm$; JCPDS No.75-1750, a = b = 0.45937 nm and c = 0.29587 nm) [20]. Among the three phases of TiO_2, rutile phase has a highest refractive index, large birefringence, and high dispersion. These properties are quite useful for the manufacturing of photovoltaic devices. The calculated lattice mismatches between tetragonal crystal structured FTO substrate ($P4_2/mnm$; JCPDS file no: 77-0452, a = b = 0.47538 nm) and deposited tetragonal rutile TiO_2 samples are; A) 5.3%, B) 4.2%, C) 4.9% and D) 5.1%. These small lattice mismatches might have promoted epitaxial nucleation of rutile TiO_2 nanoparticles on FTO substrate. The predominant peak along (101) plane observed for all samples reveals the crystallites are oriented with (101) plane. The growth rate of different crystal facets of TiO_2 follows the sequence as (110)<(100)<(101)<(001) [1]. Since the lower surface energy facet has the highest growth rate, it is expected that the crystallites to be oriented along (002) plane [16]. In FTO substrates, FTO crystallites are predominantly oriented along (101), (200) and (211) planes (Fig. 1s). Due to the small lattice constant mismatches between TiO_2 and FTO as well as the greater growth rate in (101) facet of TiO_2 on (101), (200) and (211) facets of FTO, the crystallites are predominantly oriented along (101) plane [21]. The absence of impurity peaks of phases confirms the synthesized nanostructured TiO_2 is of high crystalline quality. GIXRD pattern of sample A, for TTIP quantity of 0.05 ml shows the peaks of mixed TiO_2 and FTO. The FTO peaks do not appear in samples B, C and D. This may be due to the porous nature of nanostructures and exposed surface area of the substrate. The calculated crystallographic parameters of samples from the GIXRD patterns are given in Table 1.

3.2. Surface morphology by FESEM

FESEM images of the prepared samples for a different volume of TTIP can be seen in Fig. 2. The scanning electron micrograph of the sample for 0.05 ml of TTIP (Fig. 2a) shows the surface is mixed with nanowires, nanorods, and nanopillars of different sizes. While increasing the volume of TTIP equal to and above 0.10 ml, nanowires and nanorods were disappeared, and only nanopillars are visible on the surface. This is because of increasing growth by increasing numbers of source atomic species in the precursor concentration, and the FESEM images of these films show the surface of FTO substrate is densely packed with uniform pillar-like arrays of TiO_2 nanostructure. Further careful examination, it is observed that each pillar is consisting with a number of small, homogeneous and rectangle-shaped TiO_2 nanostructures which resemble nanorods. From the inset of Fig. 2d, the nanorods like rectangular shaped growth units orient in vertical, horizontal direction and entangled together to form nanopillar. This type of structure is new, and one could hardly see in literature.

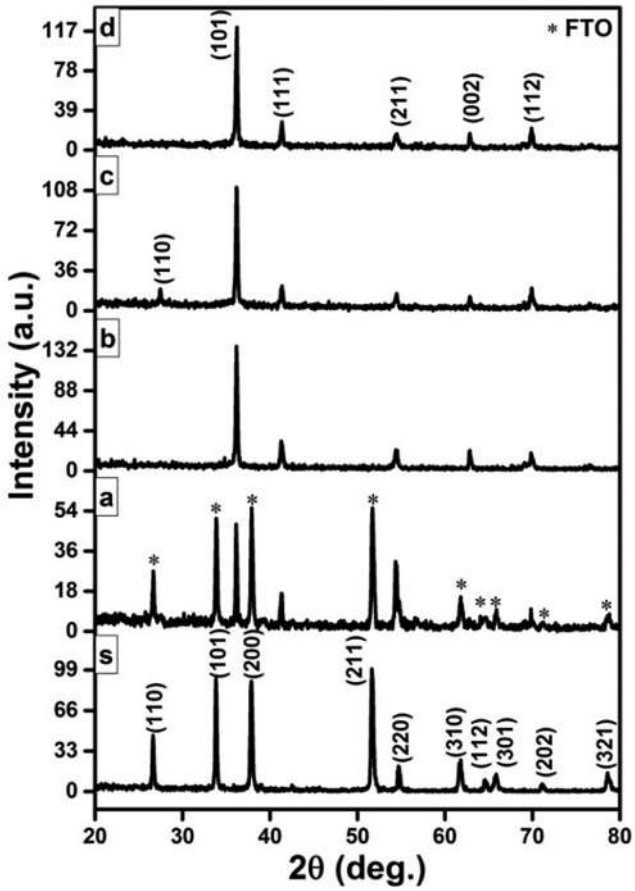

Fig. 1. GIXRD pattern of FTO substrate and prepared thin film samples. s) FTO substrate, a) 0.05 ml, b) 0.10 ml, c) 0.15 ml, and d) 0.20 ml of TTIP.

Table 1
Structural parameters calculated from GIXRD patterns.

Sample code	Crystallite size (nm)	Interplanar spacing (Å)	a (Å)	c (Å)
A	14.66	2.483	4.50	2.74
B	13.03	2.481	4.55	2.90
C	12.49	2.480	4.52	2.50
D	10.71	2.480	4.51	2.80

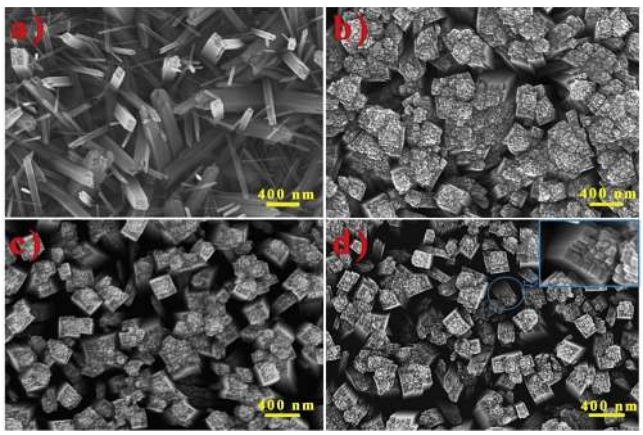

Fig. 2. FESEM images of prepared TiO_2 nanostructure. a) 0.05 ml, b) 0.10 ml, c) 0.15 ml, and d) 0.20 ml of TTIP. Inset of d is the enlarged view of a single nanopillar.

3.3. Growth mechanism

Material quality and structure depend on the parameters such as temperature, pressure, concentration, volume of precursor and pH value of precursor solution in the hydrothermal method of growth. Initially, the experiments were conducted by using glass and FTO substrates. It assured, TiO_2 molecules did not adhere to glass substrates and it well adhered on FTO substrates, which inferred the surface of FTO substrate is playing a vital role in TiO_2 nanostructure growth. From the GIXRD analysis, the maximum lattice mismatch between FTO and deposited rutile TiO_2 is 5.3%. Hence it confirmed the FTO substrate promoted the nucleation of TiO_2 crystals.

At the preparation of TiO_2 thin films, the source of Ti (TTIP) was mixed with the mixture of DI water and concentrated HCl. HCl was used to have acidic nature with a pH value of 1 which favors the slower growth rate by controlling the hydrolysis of TTIP. The experiments were conducted for 0.05 ml of TTIP at 2 h, 4 h, 6 h and 8 h duration to understand the growth mechanism. More details of as-prepared nanostructures obtained by FESEM analysis are presented in Fig. 3 respectively. The surface of the sample deposited at 2 h time period (Fig. 3a) is filled with stable shaped tent-like grains which may be originated due to lattice mismatches of TiO_2 crystals with FTO to minimize its surface energy [22]. The FESEM image of sample deposited at 4 h (Fig. 3b) is obtained with consisting white spots on the surface of saturated nanotent grains. Further, nucleated crystal growth is prolonged at an angle related to the face of tent grain and elongated as nanorods with a diameter of 53 nm in 6 h growth (Fig. 3c). Few numbers of nanorods were originated on each tent grain in 6 h, and the numbers are significantly increased in 8 h growth (Fig. 3d). Consequently, the nanopillar structures have been observed in 6 h depositions and 8 h depositions. Even so the density of nanopillars is increased in 8 h depositions compared to 6 h depositions. Fig. 4 depicts a schematic of the formation of nanopillar from nanorods. Each nanorod is formed individually on the surface of tent grain and when the deposition rise up to 8 h, the nanorod bundle is growing to become nanopillars. The growth is increased with increasing deposition time and nanorods are coalesced together to become larger diameter related to the size of tent. In general, the surface of nanomaterials is left with unbonded atoms [23], which lead to increase the surface energy of nanorods. Due to lowering the surface energy the surface atoms of nanorods could be bonded together laterally to increase in size and form nanopillar structure eventually. The average diameter of nanopillar increases with increasing growth time due to increasing in growth species.

3.4. Growth on concentration of TTIP

Surface morphological parameters such as total number of nanopillars, the average face area of nanopillars, average number of nanorods in nanopillar and the average size of nanorods are investigated from FESEM images (Fig. 2a–d) and the data are shown in Table 2. The detailed study of morphology and the growth mechanism on volume of TTIP are schematically represented in Fig. 5. Different TTIP volume is found to be a key factor to affect the parameters except for the size of nanorods (53 nm). The total number of nanopillars and the face area of nanopillars are increased with increase in TTIP volume. These variations are due to increasing the volume of TTIP enhances the number of source ions in a growth medium which might have increased the number of nucleation centers on the FTO substrates. It could have reduced the size of tent structure and

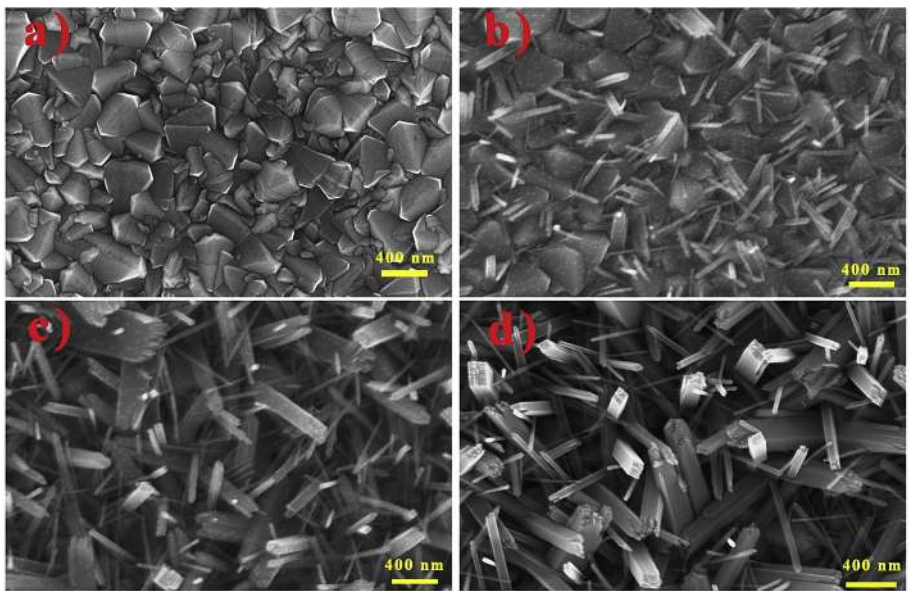

Fig. 3. FESEM images of the growth mechanism of TiO_2 nanopillars on FTO substrate at 0.05 ml TTIP with different deposition time. a) 2 h b) 4 h c) 6 h and d) 8 h.

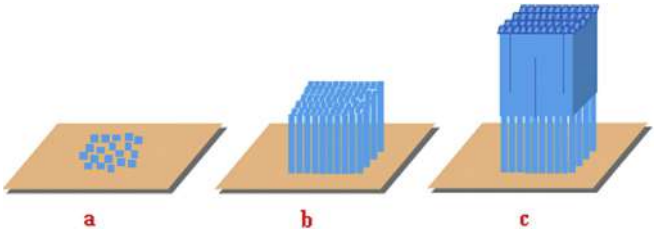

Fig. 4. Schematic representation for the formation of TiO_2 nanopillar from nanorods. a) Nucleation on nanotent surface, b) growth of nanorods and c) formation of nanopillar.

Table 2
Surface morphological parameters calculated from FESEM images.

Sample code	Total number of nanopillars at 108 μm^2 area	Average face area of nanopillars (nm^2)	Average Number of nanorods in nanopillars	Average size of nanorod in nanopillars (nm)
A	57	11531.25	91	53
B	69	72562.05	347	53
C	95	81031.25	353	53
D	107	84687.05	447	53

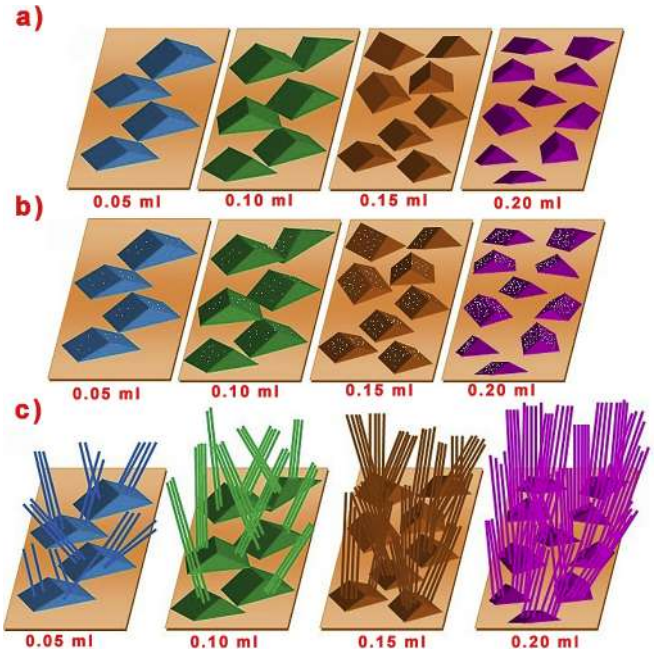

Fig. 5. Schematic diagram of the Formation of a) TiO_2 nanotent grains at 2 h with different volume of TTIP, b) Formation of nucleation centers on TiO_2 nanotent grains at 4 h of deposition with different volume of TTIP and c) Formation of TiO_2 nanopillars from TiO_2 nanorods on TiO_2 nanotent grain at 8 h of deposition with different volume of TTIP.

increase the number of tent grains as well as proposed in Fig. 5a. The average numbers of nanorods embedded in a nanopillar are increased from 91 to 447 for the amount of TTIP 0.05 ml–0.20 ml. It displays, with increasing TTIP concentration the number of nucleation centers has been increased on the tent grain (Fig. 5b) and this leads to enhances the number of rods (Fig. 5c) formed on it. The same is coalesced further and became nanopillars with increased size. Apparently, the surface area of the nanopillar will increase when its size increases.

3.5. Structure and morphological studies by AFM

Fig. 6 shows AFM images of prepared nanostructure thin films with different volume of TTIP. FTO surface is not entirely occupied by nanorods in the sample 0.05 ml of TTIP (Fig. 6a). On increasing the volume of TTIP enhances the density of

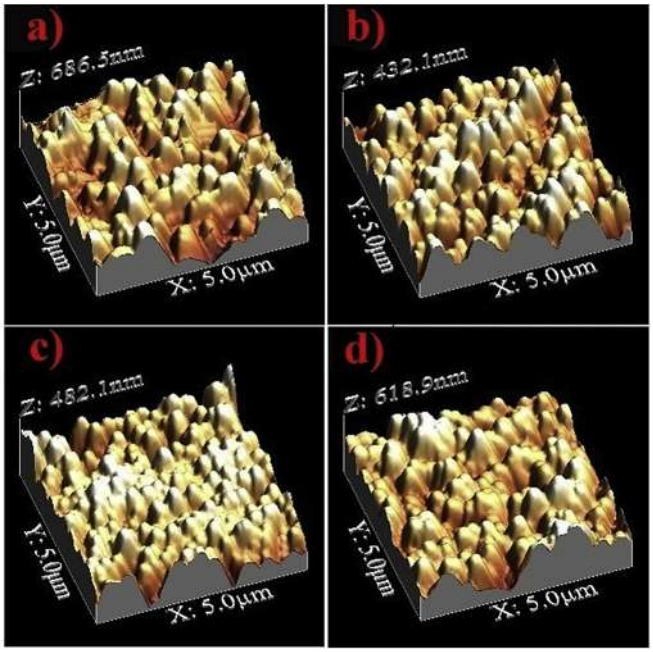

Fig. 6. AFM images of prepared TiO_2 nanostructure. a) 0.05 ml, b) 0.10 ml, c) 0.15 ml, and d) 0.20 ml of TTIP.

nanorods (Fig. 6b–d). The coalescence of nanorods to make nanopillars is clearly demonstrated in Fig. 6d. Mean square surface roughness values were calculated by using WSxM software, and it displays, increasing with TTIP volume the roughness values are decreases from 110 nm to 69 nm (Fig. 7). AFM images visualized the density of nanorods at 0.05 ml TTIP is less and subsequently, increases with increasing the TTIP volume. It is evidencing that increasing the population of nanorods by increasing TTIP volume decreases the roughness values of the films due to decreasing of voids between the nanorods/nanopillars.

3.6. Raman spectra analysis

Raman scattering spectroscopy analysis in Fig. 8 confirms the formation of rutile phase TiO_2 of the space group $P4_2/mnm$, which has six atoms in the primitive cell. The Group theory exhibit, rutile phase TiO_2 have 15 (3N-3) vibration modes which can be irreducibly represent as $A_{1g} + A_{2g} + A_{2u} + 2B_{1u} + B_{1g} + B_{2g} + E_g + 3E_u$ [24]. Here A_1g, B_{1g}, B_{2g}, and E_g are Raman-active modes. The Raman spectra of entire TiO_2 samples exhibit four peaks. Three of them are Raman active modes appeared at 143 cm^{-1}, 441 cm^{-1} and 607 cm^{-1} attributed to B_{1g}, E_g, and A_{1g} [25]. One more peak observed at 235 cm^{-1} denote disordered rutile lattice [26]. The growth of TiO_2 nanopillar takes place by the alignment of lattices in horizontal as well as in vertical direction with the adjacent lattice due to lattice orientation effect. The FESEM micrograph describes more growth units are disordered at the formation of nanopillars. Hence the peak at 235 cm^{-1} has appeared due to these disordered TiO_2 lattices. The intensity of peaks increased, owing to the average numbers of nanopillars and nanorods were increased with increasing the amount of TTIP (FESEM images and Table 2) and this would cause to promote more photons scattering.

3.7. Optical studies

PL spectra of prepared films at different amount of TTIP are shown in Fig. 9. Near band edge emission (NBE) is observed around 383 nm (3.2 eV) for all the samples [27]. Inset of Fig. 9 displays the slight blue shift in NBE peak was not found considerable variation with the increase in the volume of TTIP from 0.05 ml to 0.20 ml. In general, emission at higher energy comes from the band edges and the emission greater than the band gap energy of the material is not possible. The energy at NBE must be equal to the bandgap energy of the material; here it is almost same and not varied considerably with an increase in TTIP volume [28]. The growth units with a constant diameter of 53 nm might be the reason for constant bandgap values. The intensity of NBE for the sample prepared at 0.05 ml TTIP is greater than the samples prepared at higher volumes. The sample with 0.05 ml of TTIP evidence nanowires, nanorods, and early stage of nanopillars in FESEM image (Fig. 2a). These nanowires (2.6 nm), nanorods (53 nm) and nanopillars (199 nm) are less in diameter than the nanopillars formed above 0.05 ml of TTIP. Normally, the exciton binding energy is high and thermally stable in less diameter particle i.e. in strong confinement regime and the same is decreasing with increase in particle size [29]. Though the size of the pillar is less

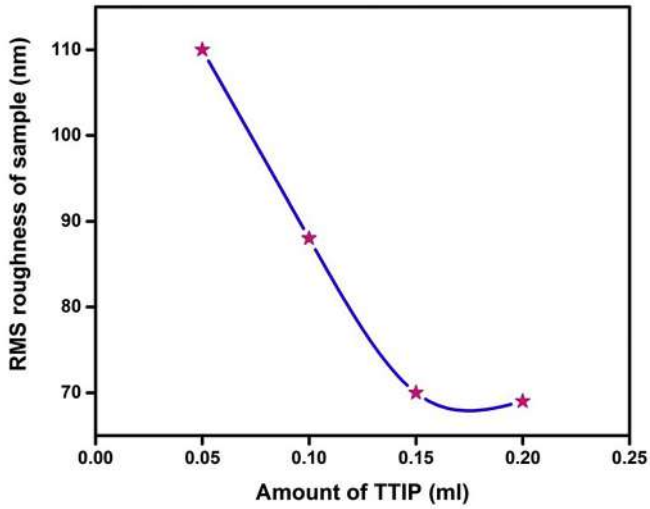

Fig. 7. Surface roughness variation of films with volume of TTIP.

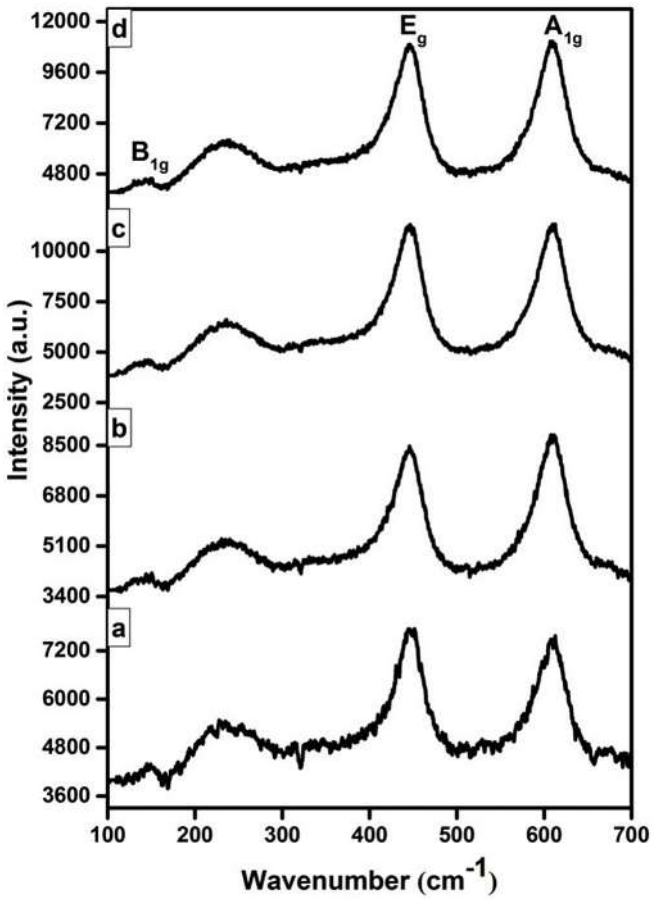

Fig. 8. Raman spectra of TiO_2 nanopillars prepared at a) 0.05 ml, b) 0.10 ml, c) 0.15 ml, and d) 0.20 ml of TTIP.

compared to other samples due to strong exciton binding energy, high-intensity NBE is observed in 0.05 ml TTIP. While increasing the amount of TTIP above 0.05 ml, the pillar size is increased so that no considerable changes in the intensity of NBE is observed. Except NBE emission, other emissions are also seen in the PL spectrum of the prepared nanostructured TiO_2. The schematic band diagram of PL emission is demonstrated in Fig. 10.

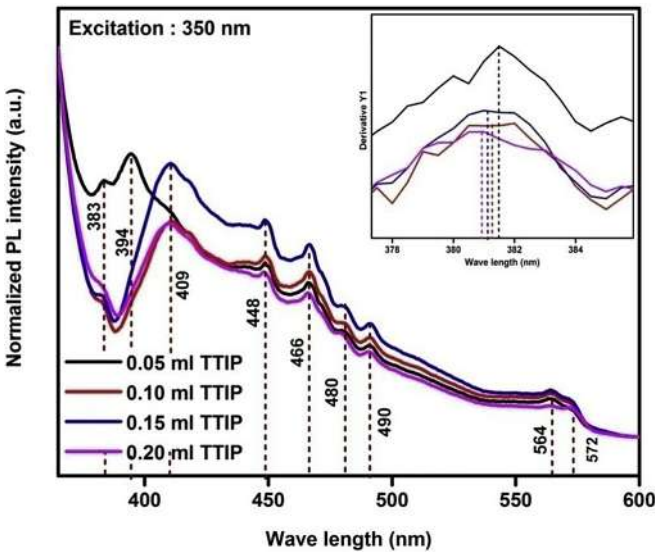

Fig. 9. PL spectra of prepared TiO_2 thin films at different volume of TTIP.

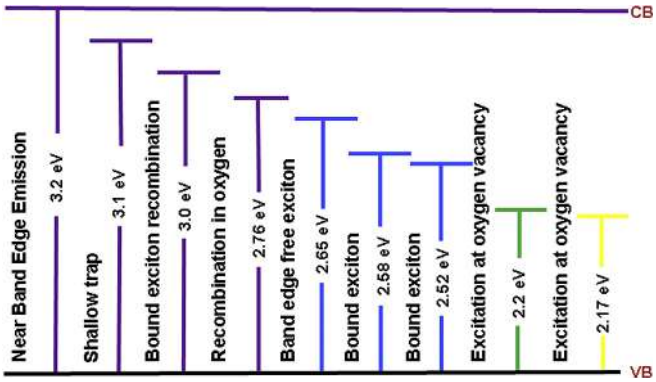

Fig. 10. Schematic band diagram of TiO_2 nanostructure from PL data [30–33].

4. Conclusions

Novel TiO_2 nanopillars were successfully synthesized on FTO substrate by the simple hydrothermal method. GIXRD patterns confirmed that synthesized TiO_2 thin films are single crystalline in nature and crystallized in rutile phase. The small lattice mismatch between rutile TiO_2 and FTO promotes epitaxial nucleation of TiO_2 tent grains on FTO surface. From the FESEM images revealed that FTO surface is uniformly and densely filled with TiO_2 nanopillars. Each nanopillar is consisting with numbers of homogeneous nanorods with 53 nm in diameter. These nanorods are orients in vertical and horizontal direction due to lattice orientation effect and forms nanopillars. It is evident of merging nanorods into the novel structure by lattice orientation effect. This novel structure is new one could hardly see anywhere. The growth mechanism of nanopillar is systematically studied from the primary nucleation with the support of FESEM and AFM images. Emission and defect energy levels are studied using PL spectra. It depicts that the near band edge emission is observed around 3.2 eV. It does not seem to vary on the TTIP volume.

References

[1] Akshay Kumar, Anuj R. Madaria, Chongwu Zhou, Growth of aligned single-crystalline rutile TiO_2 nanowires on arbitrary substrates and their application in dye-sensitized solar cells, J. Phys. Chem. C 114 (2010) 7787–7792.
[2] Jin-Yun Liao, Bing-Xin Lei, Hong-Yan Chen, Dai-Bin Kuang, Cheng-Yong Su, Oriented hierarchical single crystalline anatase TiO_2 nanowire arrays on Ti-foil substrate for efficient flexible dye-sensitized solar cells, Energy Environ. Sci. 5 (2012) 5750–5757.
[3] Hui Tong, Miki Inada, Yumi Tanaka, Naoya EnoMoto, Junichi Hojo, Preparation of nanocrystalline ZnO/TiO_2 film and its application to dye-sensitized solar cells, Funct. Mater. Lett. 5 (2012) 1–5.

[4] B. Karunagaran, Periyayya Uthirakumar, S.J. Chung, S. Velumani, E.-K. Suh, TiO_2 thin film gas sensor for monitoring ammonia, Mater. Charact. 58 (2007) 680–684.
[5] Sergiu P. Albu, Andrei Ghicov, Jan M. Macak, Robert Hahn, Patrik Schmuki, Self-organized, free-standing TiO_2 nanotube membrane for flow-through photocatalytic applications, Nano Lett. 7 (2007) 1286–1289.
[6] Bussarin Ksapabutr, Worrasit Thong-Oun, Manop Panapoy, Morphology of nanostructured TiO_2 thin film: synthesis by electrostatic spray deposition technique and its photocatalytic activity, Funct. Mater. Lett. 2 (2009) 179–183.
[7] J.E. Boercker, E. Enache-Pommer, E.S. Aydil, Growth mechanism of titanium dioxide nanowires for dye-sensitized solar cells, Nanotechnology 19 (2008) 1–10.
[8] Yulong Zhao, Xiuquan Gu, Yinghuai Qiang, Influence of growth time and annealing on rutile TiO_2 single-crystal nanorod arrays synthesized by hydrothermal method in dye-sensitized solar cells, Thin Solid Films 520 (2012) 2814–2818.
[9] Shuang Zhang, Xiuquan Gu, Yulong Zhao, Yinghuai Qiang, Enhanced photoelectrochemical performance of TiO_2 nanorod arrays by a 500°C annealing in air: insights into the mechanism, J. Electron. Mater. 45 (2016) 648–653.
[10] Zheng-ji Zhou, Jun-qi Fan, Xia Wang, Wen-hui Zhou, Zu-liang Du, Si-xin Wu, Effect of highly ordered single-crystalline TiO_2 nanowire length on the photovoltaic performance of dye-sensitized solar cells, ACS Appl. Mater. Interfaces 3 (2011) 4349–4353.
[11] Matt law, Lori E. Greene, Justin C. Johnson, Richard Saykally, Peidong Yang, Nanowire dye-sensitized solar cells, Nat. Mater. 4 (2005) 455–459.
[12] Kang-Jin Kim, Kurt D. Benkstein, Jao van de Lagemaat, Arthur J. Frank, Characteristics of low-temperature annealed TiO_2 films deposited by precipitation from hydrolyzed $TiCl_4$ solutions, Chem. Mater. 14 (2002) 1042–1047.
[13] N.G. Park, J. Van de Lagemaat, A.J. Frank, Comparison of dye-sensitized rutile-and anatase-based TiO_2 solar cells, J. Phys. Chem. B 104 (2000) 8989–8994.
[14] B. Liu, J.E. Boercker, E.S. Aydil, Oriented single crystalline titanium dioxide nanowires, Nanotechnology 19 (2008) 1–7.
[15] Christiaan Richter, Charles A. Schmuttenmaer, Exciton-like trap states limit electron mobility in TiO_2 nanotubes, Nat. Nanotechnol. 5 (2010) 769–772.
[16] Fuwei Zhuge, Takeshi Yanagida, Kazuki Nagashima, Hideto Yoshida, Masaki Kanai, Bo Xu, Annop Klamchuen, Gang Meng, Yong He, Sakon Rahong, Xiaomin Li, Masaru Suzuki, Shoichi Kai, Seiji Takeda, Tomoji Kawai, Fundamental strategy for creating VLS grown TiO_2 single crystalline nanowires, J. Phys. Chem. C 116 (2012) 24367–24372.
[17] C. Ravidhas, B. Anitha, A. Moses Ezhil Raj, K. Ravichandran, T.C. Sabari Girisun, K. Mahalakshmi, K. Saravanakumar, C. Sanjeeviraja, Effect of Nitrogen doped titanium dioxide (N-TiO_2) thin films by jet nebulizer spray pyrolysis technique suitable for photoconductive study, J. Mater Sci. Mater. Electron 26 (2015) 3573–3582.
[18] R. Devaraj, K. Venkatachalam, K. Saravanakumar, P.M. Razad, K. Mahalakshmi, Role of hexamine: growth of multiarmed ZnO nanorods and evidence of merging due to lateral growth, J. Mater. Sci. Mater Electron 27 (2016) 12201–12208.
[19] P.M. Razad, K. Saravanakumar, V. Ganesan, R.J. Choudhary, A. Moses Ezhil Raj, R. Devaraj, M. Jithin, K. Mahalakshmi, Manju Mishra Patidar, V.R. Sreelakshmi, G. Marimuthu, C. Sanjeeviraja, Novel report on single phase $BiFeO_3$ nanorod layer synthesised rapidly by novel hot-wall spray pyrolysis system: evidence of high magnetization due to surface spins, J. Mater. Sci. Mater Electron (2016), http://dx.doi.org/10.1007/s10854-016-5911-5.
[20] Xiaoyue Wang, Hai Wang, Yu Zhou, Yong Liu, Baojun Li, Xiang Zhou, Hui Shen, Confined-space synthesis of single crystal TiO_2 nanowires in atmospheric vessel at low temperature: a generalized approach, Sci. Rep. 5 (2015) 1–7.
[21] P. Soundarrajan, K. Sankarasubramanian, K. Sethuraman, K. Ramamurthi, Controlled (110) and (101) crystallographic plane growth of single crystalline rutile TiO_2 nanorods by facile low cost chemical methods, Cryst. Eng. Comm. 16 (2014) 8756–8768.
[22] L.E. Brus, J.A.W. Harkless, F.H. Stillinger, Theoretical metastability of semiconductor crystallites in high-pressure phases, with application to β-tin structure silicon, J. Am. Chem. Soc. 118 (1996) 4834–4838.
[23] C. Kumar (Ed.), Nanomaterials, Toxicity, Health and Environmental Issues, Wiley-VCH, Verlag GmbH & Co. KgaA, Weinheim, Germany, 2006, p. 351. ISBN: 3-527-31385-0.
[24] U. Balachandran, N.G. Eror, Raman spectra of titanium dioxide, J. Solid State Chem. 42 (1982) 276–282.
[25] Toshiaki Ohsaka, Fujio Izumi, Yoshinori Fujiki, Raman spectrum of anatase, TiO_2, J. Raman Spectrosc. 7 (1978) 321–324.
[26] Y. Hara, M. Nicol, Raman spectra and structure of rutile at high pressures, Phys. Stat. Sol. B 94 (1979) 317–322.
[27] Amal. K. Ghosh, F.G. Wakim, R.R. Addiss, Photoelectronic processes in rutile, Phys. Rev. 184 (1969) 979–988.
[28] Gupta Preeti, Ramrakhiani, Influence of the particle size on the optical properties of CdSe nanoparticles, Open Nanosci. J. 3 (2009) 15–19.
[29] Prashant Kumar, Chinnadurai Muthu, Vijayakumar C. Nair, K.S. Narayan, Quantum confinement effects in organic lead tribromide perovskite nanoparticles, J. Phys. Chem. C 120 (2016) 18333–18339.
[30] Xiuli Wang, Zhaochi Feng, Jianying Shi, Guoqing Jia, Shuai Shen, Jun Zhouab, Can Li, Trap states and carrier dynamics of TiO_2 studied by photoluminescence spectroscopy under weak excitation condition, Phys. Chem. Chem. Phys. 12 (2010) 7083–7090.
[31] A. Janotti, J.B. Varley, P. Rinke, N. Umezawa, G. Kresse, C.G. Van de Walle, Hybrid functional studies of the oxygen vacancy in TiO_2, Phys. Rev. B 81 (2010) 1–7.
[32] Quanjun Xiang, Kangle Lv, Jiaguo Yu, Pivotal role of fluorine in enhanced photocatalytic activity of anatase TiO_2 nanosheets with dominant (001) facets for the photocatalytic degradation of acetone in air, Appl. Catal. B 96 (2010) 557–564.
[33] L. Kernazhitsky, V. Shymanovska, T. Gavrilko, V. Naumov, L. Fedorenko, V. Kshnyakin, J. Baran, Laser-excited excitonic luminescence of nanocrystalline TiO_2 powder, Ukr. J. Phys. 59 (2014) 246–253.